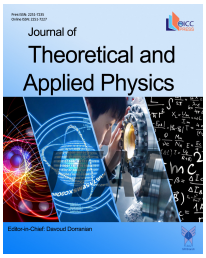

Volume 18, Issue 3, 182440 (1-8)

Journal of Theoretical and Applied Physics (JTAP)

https://dx.doi.org/10.57647/j.jtap.2024.1803.40

Emission spectroscopy of induced plasma of Au and Ag nanoparticles prepared by laser ablation in liquids

Baraa Hussam Ali*, Lazem H. Aboud, Mohammed J. Jader

Laser Physics Department, College of Science for Women, University of Babylon, Iraq.

*Corresponding author: baraahussam886@gmail.com

Original Research

Received:
4 February 2024
Revised:
30 March 2024
Accepted:
4 April 2024
Published online:
25 May 2024

Abstract:

In this study, gold and silver nanoparticles (Au NPs, and Ag NPs) were prepared by laser ablation in water using Nd:YAG laser at wavelength is 1064 nm, 1 Hz frequency. The prepared nanoparticles were deposited on a silicon wafer of (100) direction by dip coating technique. The FE-SEM results showed the nanoparticles that the spherical shapes with the average size (13.9, 12.09) nm and The structural properties were identified using the XRD results were showed the crystal size that were (10.9, 12.1) nm for each of the Au NPs, Ag NPs, respectively.

The plasma parameters were studied from the emission spectra such as temperature, Debye length, and electron density, and there were some differences between the bulk target and the nano-enhanced target. The results showed some differences in the peaks of atomic transitions in terms of intensity. The variation in the mechanism of laser-matter interaction with exist of the nanoparticles causes to enhances the emission line more than two folds. The generation mechanism of seeds electron may reduce the breakdown threshold, so increase the intensity of characteristics lines and enhance the LIBS detectability, especially for the wavelength range from 400 to 550 nm. Both plasma number density and plasma temperature increased nano-enhanced plasma by Au NPs or Ag NPs compared with the bare surface. It is possible to benefit from the improvement in some optoelectronic applications.

Keywords: NELIBS; Plasma parameters; Laser ablation method

1. Introduction

Solids, liquids, and gases can be analyzed with the use of the laser induced breakdown spectroscopy (LIBS) method in numerous applications include contamination detection [1], environmental monitoring [2], material analysis [3], food authentication [4], etc. In LIBS, plasma generated by a laser beam focused on the target material's surface excites and ionizes it. Immediately following the photons from the laser beams striking the surface of the target, plasma is emitting from the surface material. Some atomic and molecular species can be optically detected by examining the spectra of emission from laser-induced plasma [5]. The selected experimental parameters, including the target type and qualities, target type and properties, ambient gas pressure, laser light wavelength, laser pulse energy, pulse duration, and observation time duration, have a significant impact on the analytical effectiveness of LIBS [6]. A spectrometer is used to analyze the emitted radiation from plasma column. The obtained plasma spectrum provides quantitative and qualitative data such as the target composition [7]. The emission lines intensity and broadening of specific wavelengths provide information about plasma temperature and electron density [8]. According to the assumption of locally thermodynamic equilibrium, the intensity distribution of the spectral lines be obeying to Boltzmann distribution principle. So, the plasma temperature (T_e) is overrule the existence states in each level. In addition, the probability of transitions (A_{ji}), and the statistical weight of the excitation level (g_j) also effect the lines intensity, as [9]:

$$I_{ji} = \frac{N}{U(T)} g_j A_{ji} h\nu_{ji} e^{-\frac{E_j}{k_B T_e}} \quad (1)$$

where E_j is the upper level energy. By taken the natural logarithm for both sides, this relation converted to so called Boltzmann-Plot [10]. The temperature of plasma is calcu-

lated from spectral lines using the emitted lines of a selected species from the inverse of the slope of the linear relation between left hand side against the upper level energy [11]:

$$\ln\left[\frac{\lambda_{ji}I_{ji}}{hcA_{ji}g_j}\right] = -\frac{1}{k_BT_e}(E_j) + \ln|\frac{N}{U(T)}| \quad (2)$$

where: λ_{ji} and I_{ji} are the wavelength and line intensities. N and $U(T)$ represent the density of states of the emitted species, and partition function, respectively.

The Stark effect is significant in the case of the laser induced plasma by the electric field generated by the plasma sheath around ions. So, the number density of electrons can be calculated through the following relationship [12].

$$n_e = \left(\frac{\Delta\lambda}{2\omega}\right) \times N_r \quad (3)$$

where ω, and N_r represent the electron impact factor and electron density from previously determined data for a specific transition, respectively.

The plasma frequency is set so that any perturbation of the plasma's semi-neutral equilibrium produces electric fields; this frequency, which is exclusively dependent on plasma density, is one of the most essential plasma parameters which estimated by the following equation relationship [13]:

$$\omega_p = \sqrt{\frac{n_e e^2}{m_e \varepsilon_0}} \quad (4)$$

where m_e is the mass electron of electron, ε_0 is vacuum permittivity.

The Debye length (λ_D) is one of fundamental property of plasma behavior, describing the range of plasma shielding itself from an external electric field by rearrange the nearby charged particles, which leads to the generation of an opposite field that blocks the field. As seen in the following equation, the Debye length is directly proportional to square root of the electron temperature over electron density.

$$\lambda_D = \sqrt{\frac{\varepsilon_0 k_B T_e}{n_e e^2}} \quad (5)$$

The Debye length λ_D must be very little when comparing with plasma dimension to achieve the quasi-neutrality ($\lambda_D \ll L$).

Other plasma criteria say that there must be many electrons inside a "Debye sphere" to fulfill the collective behavior condition:

$$N_D = \frac{4\pi n_e}{3}\lambda_D^3 \gg 1 \quad (6)$$

The major goal of this study is to study different spectral properties of nanomaterial using LIBS techniques to calculation of plasma parameters for optical emission spectra of gold nanomaterial's.

In plasma-matter interaction differ for nanoparticles due to their different characteristics. As nearly isolated thermally system of Nano scale structures, so might increase the ablation efficiency due to rapidly rising their temperature to evaporation point [14]. As a result, surface nanoparticles can reduce the breakdown threshold causing more ablation process [15]. On the other hand, the interaction of electric fields with the plasmonic particles can cause to emit electrons by different technique of field effect from the surface as a result of local enhancement in the electromagnetic field of the incident radiation. These electrons act a started seeds for plasma breakdown [16].

Aglio et al. (2018) [17] investigated on the fundamental of enhancement mechanisms of LIBS by utilizing NPs. On various samples, including metals, transparent substances, and biological fluids, the interaction of high-intensity lasers with metal substrates and the laser-ablation processes boosted by nanoparticles were studied. Sherbini et al. (2019) [18] investigated on the signals improvement of LIBS by different types of metal NPs by using Nd:YAG laser. They examined the influence of NPs size, laser wavelength and energy to generate best signals compare with bulk samples. Quantitative modeling infers improved detectability of atomic species in biological and chemical samples. Hameed et al. (2022) [19] studied the emission lines of LIBS from three metallic targets (Cu, Ti and Ni) with laser pulses of 70 MW laser power in air. The electron temperature was determined using the ratios method, which in the ranges of $0.34-0.44$ eV, $0.28-0.42$ eV, and $0.34-0.45$ eV for Cu, Ti, and Ni respectively.

Khan et al. (2022) [20] employed the NELIBS technique to study the distinguishability of spectral lines. A colloidal of Cu NPs was generated by pulsed laser ablation in distilled water and dried on the Al surface. The study was investigated with different laser intensity and NPs concentration in unit area. The optimal NPs concentration and laser influence was 45 μL/cm^2, and 28.3 GW/cm^2 respectively.

In this work, we study the effect of plasmonic metal nanoparticles to enhance the plasma characteristics induced by pulsed laser from Si targets which can be usefull in some optoelectronic applications.

2. Materials and methods

Nd:YAG laser had a fundamental wavelength of 1064 nm, a pulse width of 10 ns, and repetition frequency of 4 HZ. Pulse energy of 100 mJ were employed in the LIBS for plasma emission spectra from Au. The pulsed laser was focused on the sample using the fluorescence lens, with a focal length of (10 cm) to reduce the incoming spot diameter from 5 mm from the laser head to 0.027 mm on the sample. The target was situated inside the sample holder at the focal point of the lens. The optical fiber was positioned and configured so that it made an angle of 45° with the laser axis at a distance of 5 cm from the sample. The aperture of the optical fiber has a diameter ($NA = 0.22/200$ m), and a lens at the intake of the fiber gathers and concentrates the plasma emission into it. The plasma emission fibers are then presented to the slit within the spectrum analyzer model (Spectra View 2100), using a silicon Charge-coupled device (Si-CCD), which consists of a number of detectors to record spectral lines with (600 Lines/mm) notches. The detected light turned into digital signals. The spectra was captured with a 0.8 nm precision spanning at the wavelength range of $(200-900)$ nm as demonstrated in Figure 1. The accuracy of all spectrum data was checked using the

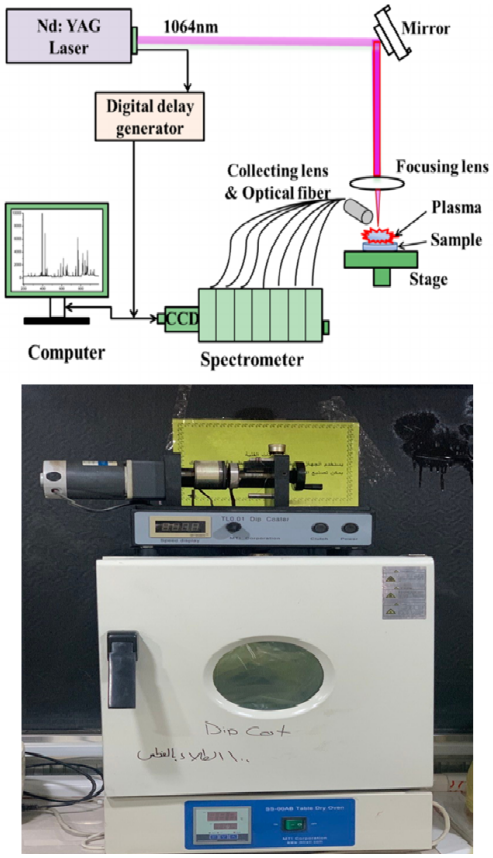

Figure 1. (a) schematic diagram of a Laser induced break down spectroscopy (LIBS) [12], (b) Dip-Coatng device .

NIST database.

The Au and Ag nanoparticles are created through the process of laser ablation in distilled water using the nano pulsed laser to the pure gold target. We noticed that the colloidal solution may have been due to the synthesis of the nanomaterial by the scraping process and the color of the deionized water turned purple. The suspension samples of Au NPs were deposited the solution containing the nanoparticles on a silicon base with a diving device as shown in Figure 1(b). Precipitated thin films are prepared by the dipping method, after preparing the nanoparticle solution, the base (silicon) is immersed in the solution for 120 seconds and extracted for 60 seconds at a temperature of 80 °C, and we repeat several times to obtain a deposited film of gold nanoparticles on silicon a sample with a film thickness of around 200 nm. This process was repeated with the generated from the silver bullion process.

3. Measurements and results

The optical absorbance spectra of the Au NPs, an Ag NPs suspensions in distilled water prepared by 400 pulses of fundamental wavelength of Nd:YAG laser were shown in Figure 2. The absorption pattern for Au NPs shows a plasmonic broad peak at 525 nm, while the plasmonic band foe the Ag NPs appeared at 400 nm wavelength, which are the characteristics local surface plasmon resonance LSPR of Au NPs and Ag NPs, respectively. These absorption bands due to the interaction of incident electromagnetic wave with the confined oscillated charged within nan orange. The band broadening indicate on wide range of nanoparticle size distribution [21].

The FE-SEM images displays in the Figure 3 at two magnification powers of 50.0 kX and 200.0 kX, for the Au NPs, Ag NPs deposited on Si wafer. The Au NPs appeared to have spherical shapes which had almost the same size uniformly deposited on the substrate. The Ag NPs also have spherical shapes of about 12 nm diameter, but aggregate to each other forming accumulations of about 200 nm diameter. These aggregations were occurred due to the oxidization capability of silver metal Also, the nano samples appeared to have almost spherical structures.

Figure 3 shows the granulate cumulating distribution number percentage for the diameters of Au NPs, Ag NPs deposited on Si wafer determined by Image J software. The spherical shapes of Au NPs have uniformly sprayed over the surface of narrow distribution from 13 to 29 nm with an average diameter of 19.49 nm. Wide particle size distribution appeared for the Ag NPs spread from 13 to 39 nm.

In order to evaluate the structural properties of the prepared nanoparticle sample, a nondestructive analytical technique of X-ray diffraction (XRD) was employed. The XRD patterns for Au NPs, and Ag NPs, deposited on a (100) Si wafer were shown in Figure 4. Polycrystalline structure with four peaks for each sample located at diffraction angles of $2\theta = 38.3301°$, $44.3124°$, $64.5285°$, and $77.5933°$ corresponding to crystalline planes (111), (200), (220), and

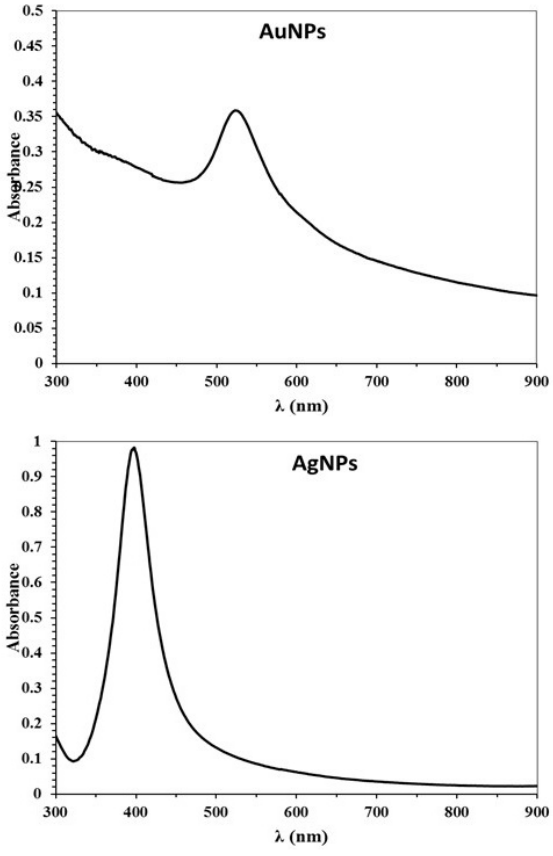

Figure 2. UV-VIS absorbance for Au NPs and Ag NPs suspension in distilled water.

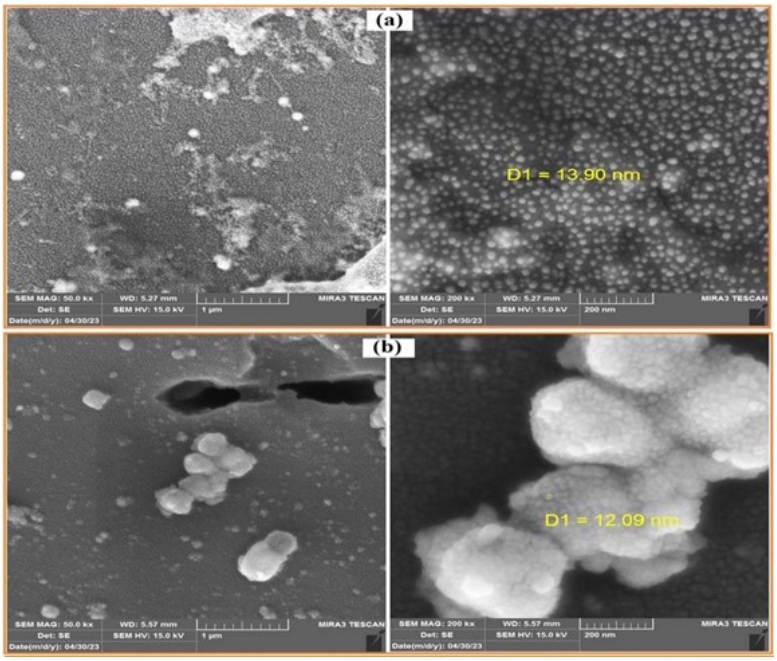

Figure 3. Represents of FE-SEM Images for(a)Au NPs, (b) Ag NPs on Si.

(311) according to JCPDF No. 96-901-2954 and 96-901-2432 standard cards. The addition intense diffraction peak corresponding to the (400) Si substrate located at diffraction angle 69°. The Ag/Si and Au/Si XRD diffraction peak positions are similar, and the Au could not be separated from metallic Ag by this XRD characterization; this is the same as the source when comparing the data [22].

The interspacing of crystalline planes d_{hkl} wad determine according to Bragg's law, while the crystallite size determine according to Shcerrer's formula [23], as listed in Table 1.

Figures 5 and 6 show a comparison between emitted spectra for LIBS from bare Si target with that coated by the two types of metal nanoparticles Ag NPs, and Ag NPs, respectively.

By using the Boltzmann plot method, which was employed in this study, the emission spectrum of the element Si II from Si Au-coated, Si Ag-coated, Si was obtained with seven values that were chosen for their high intensities and compared with the NIST database [24]. Based on this information, Table 3 was used to calculate the plasma parameters, including electron temperature, plasma frequency, electron density, Debye length, and the number of particles in the Debye sphere.

The emitted lines were matched with the atomic and ionic lines for Si (Si I, and Si II) and for the two used metals. It is clear that the intensity of the lines is higher and more distinguishable for samples coated by the two types of nanoparticles, especially within the range from 400 to 550 nm, compare with the bulk Si targets. As an example, the Si II (504.1 nm) line enhanced in intensity about 2.1 fold after nano enhancement by Au NPs. Also, revealing that the spectral lines be more broadening for the nano-enhanced samples, which indicates an increase in the plasma density [25].

The probability of breakdown increased as a result of reducing the breakdown threshold on the sample surface. The metal nanoparticles act as nearly as thermally insulated, so they are rabidly heated by irradiation causing evaporation or sublimation of the NPs [26].

Electron temperature (T_e) were determined by Boltzmann-Plot, as shown in Figure 7, using the intensities of Si II lines and their parameters from NIST site [26] as listed in

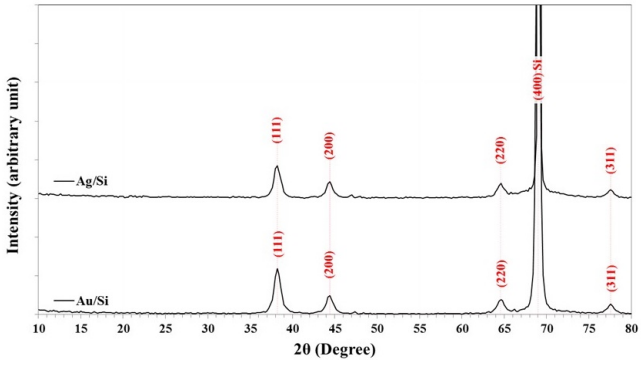

Figure 4. XRD Spectrum for gold thin film at (ELaser= 100 mJ , f = 4 Hz, No. of pulse = 600).

Table 1. XRD parameters of gold and silver nanoparticles.

Sample	2θ (Deg.)	FWHM (Deg.)	d_{hkl} Exp.(Å)	C.S (nm)	hkl
Au NPs /Si	38.3301	0.8502	2.3464	9.9	(111)
	44.3124	0.8752	2.0425	9.8	(200)
	64.5285	0.8251	1.4430	11.4	(220)
	77.5933	0.8251	1.2294	12.4	(311)
Ag NPs /Si	38.1925	0.7802	2.3545	10.8	(111)
	44.4499	0.6601	2.0365	13.0	(200)
	64.5285	0.7701	1.4430	12.2	(220)
	77.5933	0.8251	1.2294	12.4	(311)

Table 2. NIST parameters for the used emitted line for Si II in T_e determination.

Wavelength (nm)	$g_k A_{ki}$ (s^{-1})	E_i (eV)	E_k (eV)
290.569	3.06×108	9.838769	14.104461
321.003	3.17×108	10.07388	13.935169
385.602	1.76×108	6.859448	10.07388
504.103	2.80×108	10.066443	12.525262
546.643	1.30×108	12.525262	14.792721
566.956	4.00×108	14.199804	16.386036
597.893	2.26×108	10.07388	12.146991
634.710	2.34×108	8.121023	10.07388

Table 3. Parameters of plasma induced from Si target and that enhanced by Au NPs, and Ag NPs.

Target	T_e (eV)	FWHM (nm)	$n_e \times 10^{18}$ (cm^{-3})	$f_p \times 10^{12}$ (Hz)	$\lambda_D \times 10^{-4}$ (cm)	$N_d \times 10^4$
Si	3.958	2.500	1.042	9.165	0.145	1.33
Au-coated Si	4.341	3.500	1.458	10.844	0.128	1.29
Ag-coated Si	4.441	3.000	1.250	10.040	1.400	1.44

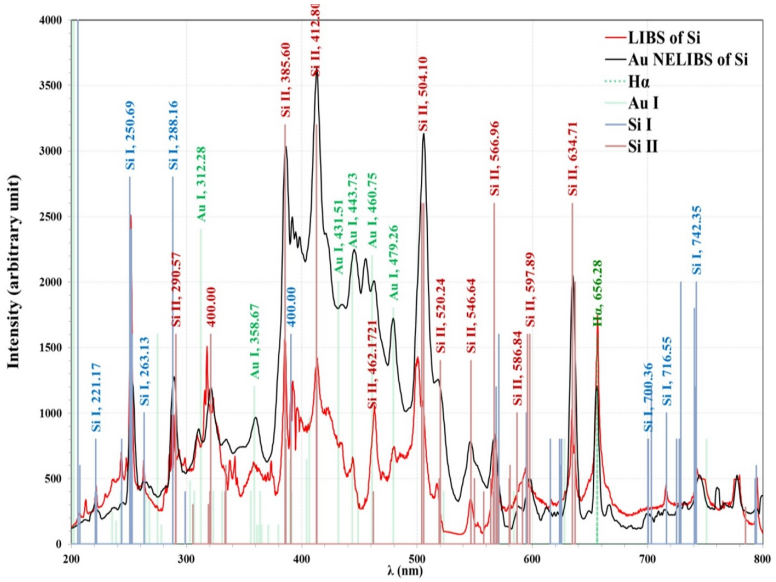

Figure 5. Comparison between the emitted spectra from bare Si target with that coated by Au NPs.

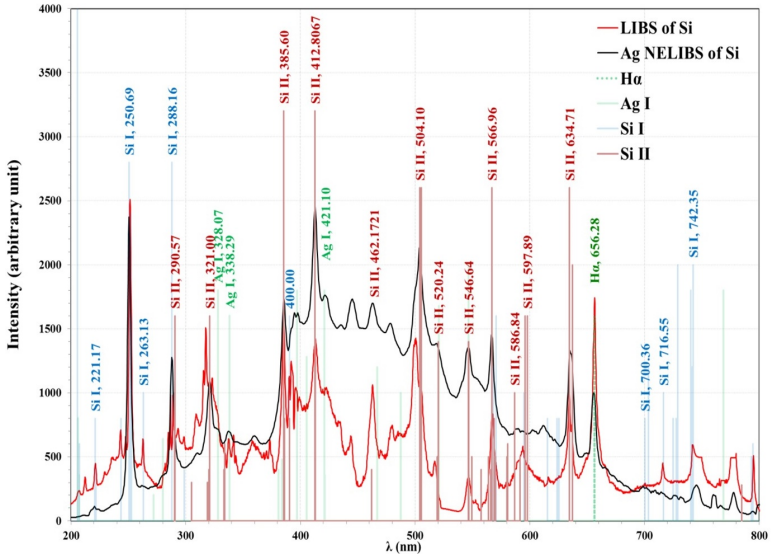

Figure 6. Comparison between the emitted spectra from bare Si target with that coated by Ag NPs.

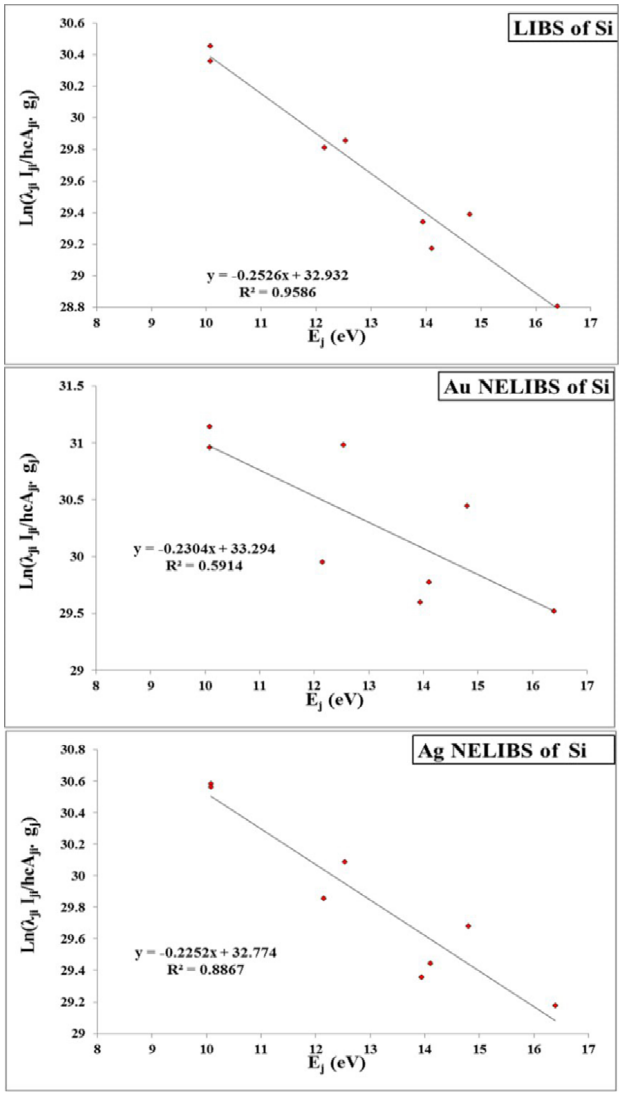

Figure 7. Boltzmann plot for LIBS from Si target and enhanced with Au NPs and Ag NPs.

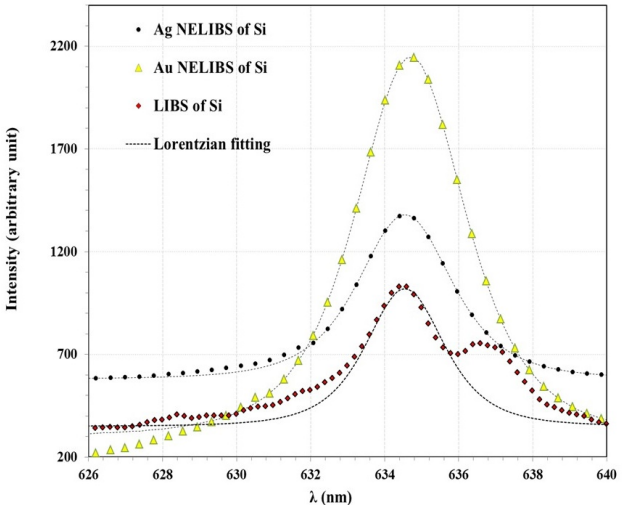

Figure 8. Lorentzian fitting corresponding to Si II (634.71 nm) line for LIBS from Si target and enhanced with Au NPs and Ag NPs.

Table 2.

Figure 8 displays the Lorentzian fitting for the Si II (634.71 nm) line for LIBS from the Si target and that enhanced with Au NPs and Ag NPs. The full width of the emitted line ($\Delta\lambda$) was taken from the best Lorentzian which was employed to determine electron number density for each case according to the data of electron impact width (ω_m) for this selected line [27].

Other plasma parameters, including plasma frequency (f_p), Debye length (λ_D) and Debye number (N_d) were calculated using the Equations (4), (5), and (6), respectively as listed in Table 3. The plasma parameters satisfy the plasma criteria. The NELIBS decrease the ionization threshold and so increases the electron density. The electron also can be emitted from samples coated by the plasmonic nanoparticles due to the interaction with laser radiation which causes emitted electrons by field effect emission. On the other hand, in-

creasing T_e is a result of enhancing energy absorption by the nanoparticles.

4. Conclusion

In the present study, we have focused on the plasma spectra which is emitted from gold and silver metals under the influence of laser pulses. In addition, the Au NPs and Ag NPs are generated experimentally by pulsed laser ablation method with nanosecond laser pulses at 1064 nm at 600 number of pulses. The results indicated obtaining quantitative plasma confinement, and thus the dimensions of the nanoparticles are very small which candidate for use in multiple scientific applications based on the plasma parameters resulting of the emission spectra. The silicon substrate have a clear effect on the results the LIBS of plasma characteristics induced by pulsed laser as a result of the variation in the mechanism of laser-matter interaction. Furthermore, the generation mechanism of seeds electron may reduce the breakdown threshold, so increase the intensity of characteristics lines and enhance the LIBS detection capability, especially for low absorption materials. Also the plasma temperature and plasma number density of silver is higher than that of gold, this is due to the wavelength of the laser used to heat metals. The FE-SEM results show of the metal nanoparticles of quasi-spherical morphology with an average size (13.20) nm. In addition, the XRD patterns show of the metal nanoparticles of polycrystalline cubic structure, as well as the average crystallite size were (10.9, 12.1) nm of the Au NPs, Ag NPs, respectively.

Authors Contributions
Baraa Hussam ali measure the samples response and write the first version of the manuscript, Lazem H. Aboud and Mohammed J. Jader, supervised the work and edit the paper in final version.

Availability of data and materials
Presented data in the manuscript are available via request.

Conflict of Interests
The author declare that they have no known competing financial interests or personal relationships that could have appeared to influence the work reported in this paper.

References

[1] Q. Zhao, Y. Yu, P. Cui, N. Hao, C. Liu, P. Miao, and Z. Li. "Laser-induced breakdown spectroscopy (LIBS) for the detection of exogenous contamination of metal elements in lily bulbs, Spectrochim.". *Acta Part A Mol. Biomol. Spectrosc.*, **287**:122053, 2023. DOI: https://doi.org/10.1016/j.saa.2022, 122053(2).

[2] Y. Zhang, T. Zhang, and H. Li. "Application of laser-induced breakdown spectroscopy (LIBS) in environmental monitoring, Spectrochim.". *Acta Part B At. Spectrosc.*, **181**:106218, 2021. DOI: https://doi.org/10.1016/jsab.2021, 106218.

[3] K. Keerthi, S. D. George, S. D. Kulkarni, S. Chidangil, and V. K. Unnikrishnan. "Elemental analysis of liquid samples by laser induced breakdown spectroscopy (LIBS): Challenges and potential experimental strategies.". *Opt. Laser Technol.*, **147**:107622, 2022. DOI: https://doi.org/10.1016/j.optlastec.2021, 107622.

[4] S. Shin, X. Wu, V. Patsekin, I.-J. Doh, E. Bae, J. P. Robinson, and B. Rajwa. "Analytical approaches for food authentication using LIBS fingerprinting, Spectrochim. ". *Acta Part B At. Spectrosc.*, **205**:106693, 2023. DOI: https://doi.org/10.1016/j.sab.2023, 106693.

[5] D. M. Wong, A. A. Bolshakov, and R. E. Russo. "Laser induced breakdown spectroscopy. ". *Encyclopedia of Spectroscopy and Spectrometry*, :533–538, 2016. DOI: https://doi.org/10.1016/B978-0-12-803224-4.00062-5.

[6] Y. Rao, T. Sun, C. Sun, and J. Yu. "A combination of spectrum selection and machine learning regression for minor element determination in gravel stones with LIBS, Spectrochim.". *Acta Part B At. Spectrosc.*, **198**:106567, 2022. DOI: https://doi.org/10.1016/j.sab.2022, 106567.

[7] A. Ahmed, M. Salman, M. Alwazzan, and A. Meri. "Blushers component analysis for unbranded cosmetic brands: Elements' concentration levels and its effect on human body.". *J. Adv. Res. Dyn. Control Syst.*, **11**:412–419, 2019.

[8] S. Zhang, X. Zeng, H. Bai, C. Zhang, and T. Shao. "Optical emission spectroscopy measurement of

plasma parameters in a nanosecond pulsed spark discharge for CO_2/CH_4 dry reforming, Spectrochim. ". *Acta Part A Mol. Biomol. Spectrosc.*, **267**:120590, 2022. DOI: https://doi.org/10.1016/j.saa. 2021, 12059.

[9] D. M. Devia, L. V Rodriguez-Restrepo, and E. Restrepo-Parra. "Methods employed in optical emission spectroscopy analysis: a Review. ". *Ingeniería y Ciencia*, **11**:239–267, 2015. DOI: https://doi.org/10.17230/ingciencia.11.21.12.

[10] T. A. Hameed and S. J. Kadhem. "Plasma diagnostic of gliding arc discharge at atmospheric pressure.". *Iraqi Journal of Science*, **60**:2649–2655, 2019. DOI: https://doi.org/10.24996/ijs.2019.60.12.14.

[11] V. Unnikrishnan, K. Alti, V. Kartha, C. Santhosh, G. Gupta, and B. Suri. "Measurements of plasma temperature and electron density in laser-induced copper plasma by time-resolved spectroscopy of neutral atom and ion emissions. ". *Pramana - J. Phys.*, **74**: 983–993, 2010. DOI: https://doi.org/10.1007/s12043-010-0089-5.

[12] X. F. Li, W. D. Zhou, and Z. F. Cui. "Temperature and electron density of soil plasma generated by LA-FPDPS. ". *Frontiers in Physics*, **7**:721–727, 2012. DOI: https://doi.org/10.1007/s11467-012-0254-z.

[13] C. Fallon. "Optical diagnostics of colliding laser produced plasmas: Towards next generation plasma light sources. PhD Thesis, Dublin City University". , 2013.

[14] D. A. Cremers and L. J. Radziemski. "History and fundamentals of LIBS". *Cambridge University Press*, **84**:1–39, 2009. DOI: https://doi.org/10.1017/CBO9780511541261.002.

[15] S. Marino, S. Palanco, M. Gabás, R. Romero, and J. R. Ramos-Barrado. "Laser nano- and micro-structuring of silicon using a laser-induced plasma for beam conditioning.". *Nanotechnology*, **26**:055303, 2015. DOI: https://doi.org/10.1088/0957-4484/26/5/055303.

[16] A. De Giacomo, R. Gaudiuso, C. Koral, M. Dell'Aglio, and O. De Pascale. "Nanoparticle Enhanced Laser Induced Breakdown Spectroscopy: Effect of nanoparticles deposited on sample surface on laser ablation and plasma emission, Spectrochim.". *Acta Part B At. Spectrosc.*, **98**:19–27, 2014. DOI: https://doi.org/10.1016/j.sab.2014.05.010.

[17] M. Dell'Aglio, R. Alrifai, and A. De Giacomo. "Nanoparticle enhanced laser induced breakdown spectroscopy (NELIBS), a first review, Spectrochim.". *Acta Part B At. Spectrosc.*, **148**:105–112, 2018. DOI: https://doi.org/10.1016/j.sab.2018.06.008.

[18] A. M. EL Sherbini, A. E. EL Sherbini, C. G. Parigger, and T. M. EL Sherbini. "Nano-particle enhancement of diagnosis with Laser-Induced plasma spectroscopy. ". *J. Phys. Conf. Ser.*, **1253**:012002, 2019. DOI: https://doi.org/10.1088/1742-6596/1253/1/012002.

[19] S. K. Hameed, N. A. Razzak, A. F. Mahood, and K. L. Nahi. "Optical emission spectroscopy of laser-produced plasmas of some metal targets. ". *Iraqi J. Appl. Phys.*, **18**:15–20, 2022.

[20] M. R. Khan, S. U. Haq, Q. Abbas, and A. Nadeem. "Improvement in signal sensitivity and repeatability using copper nanoparticle-enhanced laser-induced breakdown spectroscopy, Spectrochim.". *Acta Part B At. Spectrosc.*, **195**:106507, 2022. DOI: https://doi.org/10.1016/j.sab.2022.106507.

[21] R. Borah and S. W. Verbruggen. "Effect of size distribution, skewness and roughness on the optical properties of colloidal plasmonic nanoparticles.". *Colloids Surfaces A Physicochem. Eng. Asp.*, **640**:128521, 2022. DOI: https://doi.org/10.1016/j.colsurfa.2022.128521.

[22] J. Liu, Zh. Wu, Q. He, Q. Tian, W. Wu, X. Xiao, and C. Z. Jiang. "Catalytic application and mechanism studies of argentic chloride coupled Ag/Au hollow heterostructures: Considering the interface between Ag/Au bimetals.". *Nanoscale Research Letters*, **14**: 1–13, 2019. DOI: https://doi.org/10.1186/ s11671-019-2862-9.

[23] M. O. Salman, M. A. Kadhim, and A. A. Khalefa. "CdO: SnO_2 composite UV-assisted room temperature ozone sensor.". *Iraqi J. Sci.*, **64**:1190–1202, 2023.

[24] NIST. "Atomic Spectra Database. NIST Standard Reference Database. Version 410". ., .

[25] B. Zmerli, B. Nessib, and M. S. Dimitrijevi. "On the Stark broadening of CuI spectral lines. ". *Memorie della Societa Astronomica Italiana Supplementi*, **15**: 152–156, 2010.

[26] S. Hashimoto, D. Werner, and T. Uwada. "Studies on the interaction of pulsed lasers with plasmonic gold nanoparticles toward light manipulation, heat management, and nanofabrication. ". *J. Photochem. Photobiol. C Photochem. Rev.*, **13**:28–54, 2012. DOI: https://doi.org/10.1016/j.jphotochemrev.2012.01.001.

[27] N. Konjević and W. L. Wiese. "Experimental Stark widths and shifts for spectral lines of neutral and ionized atoms. ". *J. Phys. Chem. Ref. Data.*, **19**: 1307–1385, 1990.